Electronic Supplementary Material (ESI) for Organic Chemistry Frontiers.

SUPPLEMENTARY INFORMATION

Sensitive dipstick assays for lectin detection, based on glycan-BSA conjugate immobilisation on gold nanoparticles

Pedro J. Hernando,[1,2] Irina M. Ivanova,[1] Simona Chessa,[1] María J. Marín,[2] Simone Dedola,[1,3] Robert A. Field[1,3]*

1. Iceni Glycoscience, Norwich Research Park, Norwich NR4 7GJ
2. School of Chemistry, University of East Anglia, Norwich Research Park, Norwich NR4 7TJ
3. School of Chemistry and Manchester Institute of Biotechnology, University of Manchester, Manchester M1 7DN

Email: robert.field@manchester.ac.uk

Materials

Reagents

All reagents were of analytical grade and purchased from Sigma Aldrich, Merck, Fischer Scientific, Thermo Fischer Scientific or Carbosynth unless stated otherwise. Citrate-capped 40 nm AuNPs were purchased from Expedeon, NHS-ester-activated 40 nm AuNPs were purchased from CytoDiagnostics and NHS-activated 150 nm AuNSs were purchased from NanoComposix).

Buffers/media

A summary of the buffers and media used in this work can be found in **Table S1.**

Table S1. Buffers and media used in this work.

Buffer/media name	Composition
Citric acid buffer	2 mM citric acid buffer, pH 5.3
ConA buffer	10 mM HEPES, pH 8.5, 100 mM $CaCl_2$
Dipstick buffer (AuNPs)	PBS with 1% PVP
Dipstick buffer (AuNSs)	PB with 1% PVP, 1% BSA, 1% Triton-X100
HEPES-PEG reaction buffer	100 mM HEPES buffer (pH 8.0), 0.5% (w/v) PEG-20k
Phosphate buffer (PB)	10 mM phosphate buffer, pH 7.6
Phosphate buffer saline (PBS)	PB with 50 mM NaCl
Phosphate buffer, Tween-20 (PBT)	PB with 0.5% Tween-20
Phosphate buffer saline, Tween-20 (PBST)	PBS with 0.5% Tween-20
RCA_{120} buffer	10 mM Na_3PO_4, 150 mM NaCl, pH 7.8
UEA I buffer	10 mM HEPES, pH 7.5, 150 mM NaCl, 0.1 mM $CaCl_2$
WGA buffer	10 mM HEPES, pH 8.5, 100 mM $CaCl_2$

Instrumental techniques

A summary of the equipment used in this work can be found in **Table S2.**

Table S2. Equipment and instruments used in this work

Equipment / technique	Instrument manufacturer / model
Centrifuge	Techne Genofuge 16M microcentrifuge
Dynamic Light Scattering	Malvern Zetasizer Nano-ZS
High-Performance Mass spectrometry	Bruker Daltonics autoflex speed ToF/ToF mass spectrometer
Infrared spectroscopy	Perkin Elmer Fourier Transform Infrared spectrometer
Liquid Chromatography - Mass spectrometry	Advion Expression Compact Mass Spectrometer
Nuclear Magnetic Resonance	Bruker AVIII 400 MHz and Bruker NEO 600 MHz
Plate reader	POLARstar Omega, BMG Labtech
Polarimetry	Perkin Elmer PE 341/342
Rotatory mixer	Benchtop MX-RL-E rotatory laboratory mixer
Transmission electron microscopy	FEI Tecnai F20 S/TEM
UV-Vis spectroscopy	Hitachi U-3900 spectrophotometer

Dynamic Light Scattering

For dynamic light scattering size measurements, the sample (500 µL) in PBS was added to a 1 mL quartz cuvette. The sample was equilibrated for two minutes, and the mean average size was collected from three runs, with at least 5 measurements per run.

Infrared spectroscopy

Perkin Elmer Fourier Transform Infrared spectrometer with attenuated total reflection (ATR) attachment was used to record the IR spectra of the azide-containing compounds. If enough amount of material was available, the sample was not diluted and directly deposited on the ATR crystal. If a limited amount of compound was available, the sample was diluted in MeOH

to 10 mg/mL, from which 20 µL were deposited on the instrument glass and dried before recording the spectrum. Spectrum One software was used for data analysis.

Mass spectrometry

Electrospray ionisation mass spectrometry in positive mode was used for the characterisation of carbohydrate derivates, where necessary. A 10 µL sample at the concentration of 0.01 mg/mL were injected. Advion Mass Express software was used for data analysis.

Matrix-assisted laser desorption/ionisation time-of-flight mass spectrometry was used for the characterisation of carbohydrate-BSA conjugates. A sample containing 250 µg/mL of BSA conjugate was pre-mixed in a 1: 1 ratio with a DHB matrix. The sample was prepared depositing 1 µl of DHB matrix on an MTP AnchorChip 384 target plate and it was allowed to dry for 10 minutes. Successively, 1 µL of the pre-mixed sample-matrix sample was deposited on the plate and allowed to dry for 10 minutes. The MALDI-TOF MS equipment used a nitrogen laser, and analysis was performed in a linear 3-shot mode, with 32x gain and 70% laser intensity.

Nuclear Magnetic Resonance spectroscopy

Nuclear Magnetic Resonance equipment used a broadband BBFO probe at 400 MHz (^{1}H) and 100 MHz (^{13}C) at 298 K. Compounds were characterised using 1D-^{1}H, 1D-^{13}C, ^{1}H-^{1}H- COSY, ^{1}H-^{13}C-HSQC and ^{1}H-^{1}H-NOESY. Mestrenova software (Mestrelab Research, S.L.) was used for data analysis. For ^{13}C-NMR experiments measured in D_2O as the solvent, 10 µL of acetone were added as a reference.

Polarimetry

Perkin Elmer PE 341/342 polarimeter was used to measure optical rotation of chiral compounds. Measurements were taken at 25 ^{o}C and using the sodium D line (589 nm) as the source of light. According to the specific solubility, samples were prepared using MeOH, chloroform or water, at the indicated concentration, ranging 0 – 10 mg/mL (c = 0 – 1).

Transmission electron microscopy

For transmission electron microscopy (TEM) imaging, 400 mesh copper palladium grids with carbon-coated pyroxylin support film were used. A volume of 10 µL of the sample was adsorbed on the grid, which was allowed to dry at room temperature overnight.

The samples were submitted to the TEM facility at the University of East Anglia, where the grids were placed in the instrument, operating at 200 kV, and imaged using an AMT XR60B digital camera (Deben).

UV-Vis spectroscopy

UV-Vis measurements were obtained using a UV-Vis spectrophotometer or a plate reader. For UV-Vis spectrophotometer measurements, samples (1 mL) were added to a quartz cuvette and measured using Cary WinUV software, with a 1 cm path length. For plate reader measurements, samples (50 µL) were loaded into 384-well microtiter plates (4titude), and measurements were recorded using Omega series and MARS Data Analysis software (BMG Labtech).

Glycosides synthesis

3-Azidopropyl 2,4-di-*O*-benzoyl-3,6-di-*O*-(2,3,4,6-penta-*O*-benzoyl-α-D-mannopyranosyl)-α-D-mannopyranoside (5a)

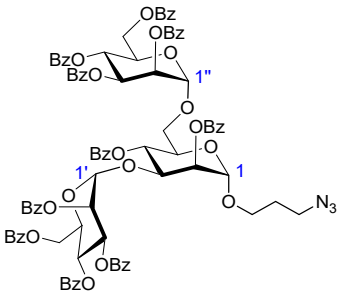

Adapted from Oscarson *et al.*[9] 3-Azidopropyl 2,4-di-*O*-benzoyl-α-D-mannopyranoside (98 mg, 0.2 mmol) and perbenzoylated mannopyranosyl bromide (502 mg, 0.68 mmol, 3.7 eq.) were dissolved in anhydrous toluene (5 mL) at -20 ºC. Silver triflate (212 mg, 0.54 mmol, 4 eq.) was dissolved in anhydrous toluene (5 mL) and added dropwise to the acceptor-donor mixture. The mixture was allowed to room temperature and stirred overnight, at which point TLC (Hex-EtOAc 7:3) showed complete conversion of the acceptor. TEA (0.3 mL) was added and the mixture was stirred for 20 minutes. The black precipitate was filtrated over celite and the solvent was evaporated under reduced pressure. Purification by flash chromatography (Hex-EtOAc 100:0 to 70:30) gave compound **5a** as a white solid (114 mg, 34%). R_f value (Hex-EtOAc 7:3): 0.40. $[\alpha]_D^{25}$ – 42.5 (*c* 1.0, $CHCl_3$)[no lit.] (see note at the end of the paragraph). δ_H ($CDCl_3$; 400 MHz): 8.33-7.20 (m, 50 H, H_{Ar}), 6.16-5.94 (m, 4H, H-4', H-4'', H-3', H-3''), 5.75-5.67 (m, 4H, H-4, H-2, H-2', H-2''), 5.37 (d, $J_{1,2}$ = 2.1 Hz, 1 H, H-1), 5.14 (app s, 2 H, H-1', H-1''), 4.64-4.57 (m, 4 H, H-6a', H-6a''), 4.52 (dt, $J_{4,5}$ = 3.0, $J_{5,6a}$ = $J_{5,6b}$ = 10.0 Hz, 1 H, H-5), 4.46 (dt, $J_{4',5'}$ = 2.7, $J_{5',6a'}$ = $J_{5',6b'}$ = 10.0 Hz, 1 H, H-5'), 4.41-4.31 (m, 4 H, H-6b', H-6b''), 4.31-4.24 (m, 1 H, H-5''), 4.17 (dd, $J_{5,6a}$ = 6.6, $J_{6a,6b}$ = 10.4 Hz, 1 H, H-6a), 4.04 (dt, $J_{7a,7b}$ = 9.7, $J_{7a,8}$ = 6.1 Hz, 1 H, H-7a), 3.78 (dd, $J_{5,6a}$ = 1.9, $J_{6a,6b}$ = 10.4 Hz, 1 H, H-6b), 3.7 (dt, $J_{7a,7b}$ = 9.7, $J_{7a,8}$ = 6.1 Hz, 1 H, H-7b), 3.56-3.46 (m, 2H, H-9), 2.06-1.96 (m, 2 H, H-8). δ_C ($CDCl_3$; 400 MHz): 166.4 (1C, C=O), 166.24 (1C, C=O), 166.24 (1C, C=O), 165.8 (1C, C=O), 165.6 (1C, C=O), 165.44 (1C, C=O), 165.42 (1C, C=O), 165.3 (1C, C=O), 164.9 (1C, C=O), 164.8 (1C, C=O), 133.—128.0 (34 x s, 60 C, C_{Ar}), 99.9 (1C, C-1), 97.8 (1C, C-1'), 97.5 (1C, C-1''), 77.0 (s, 1C, C-5), 72.1, 70.5, 70.4, 70.2, 70.0, 69.8, 69.5, 69.1, 68.6 (9 x s, 9 C, H-2, H-2', H-2'', H-3', H-3'', H-4, H-4'', H-5', C-H5''), 67.0 (s, 1 C, C-

6), 66.8 (s, 1 C, C-H-4'), 66.5 (s, 1 C, H-3), 65.5 (s, 1 C, H-7), 62.8 (s, 1 C, C-H-6'), 62.5 (s, 1 C, H-6''), 48.5 (s, 1 C, C-9), 28.9 (s, 1 C, C-8). IR (cm^{-1}): 2098.4 (N_3). MALDI-TOF: found *m/z* 1650.4656 $[M+Na]^+$, calcd for $C_{91}H_{77}N_3O_{26}Na$ 1650.4685. The $[\alpha]_D^{25}$ values reported for similar mannotriosides by Oscarson *et al.*[9] are in the -17 to -52 range, which is in agreement with the data hereby reported.

3-Azidopropyl 2,4-di-*O*-α-D-mannopyranosyl-α-D-mannopyranoside (5)

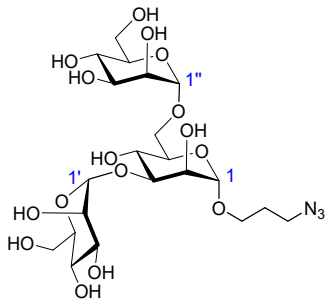

Adapted from Yu *et al.*[10] Benzoylated 3-azidopropyl mannotrioside (**5a**, 90 mg, 0.06 mmol) was dried under high-vacuum. Absolute MeOH (2 mL) and NaOMe (0.2 mL, 1 M) was added under nitrogen atmosphere. After 45 minutes, TLC (EtOAc-Hex 7:3) showed completion of the reaction. To investigate the presence of intermediate deprotected species, a more polar mobile phase was employed, consisting of IPA-NH_4OH-H_20 6:4:1. The reaction was neutralised using acidic DOWEX resin, the resin was filtered and the organic solvent was evaporated under reduced pressure. The reaction mixture was purified by gel permeation chromatography (0.5 mL/min, RT_o = 450, RT_f = 580). Accordingly, the deprotected compound **5** was isolated as a white powder (30 mg, 93%). R_f value (IPA-NH_4OH-H_20 6:4:1): 0.27. $[\alpha]_D^{25}$ – 78.2 (*c* 1.0, H_2O)[no lit.] (see note at the end of the paragraph). δ_H (D_2O; 400 MHz): 5.32(d, $J_{1'',2''}$ = 3.1 Hz, 1H, H-1''), 4.83 (d, $J_{1',2'}$ = 1.4 Hz, 1H, H-1'), 4.45 (d, $J_{1,2}$ = 7.7 Hz, 1H, H-1),4.05-3.89 (m, 3H, H-2, H-2', H-2''), 3.49-3.90 (m, 17 H, H-3, H-3', H-3'', H-4, H-4', H-4'', H-5, H-5', H-5'', H-6, H-6', H-6'', H-7), 3.41-3.35 (m, 2H, H-9), 1.88-1.79 (m, 2H, H-8). δ_C (101 MHz): 102.3 (1C, C-1), 99.9 (1C, C-1'), 99.4 (1C, C-1''), 78.4, 73.3, 72.7, 71.1, 70.6, 70.3, 66.8, 66.7, 65.7 (9 x s, 9C, H-3, H-3', H-3'', H-4, H-4', H-4'', H-5, H-5', H-5''), 70.03, 69.95, 69.7 (3 x s, 3C, C-2, C-2', C-2''), 65.3 (s, 1C, C-6), 64.9 (1C, C-7), 60.97 (1C, C-6'), 60.92 (1C, C-6''), 48.1 (1C, C-9), 27.8 (1C, C-8). IR (cm^{-1}): 2098.2 (N_3). MALDI-TOF: found m/z 610.2057 $[M+Na]^+$, calcd for $C_{21}H_{37}N_3O_{16}Na$ 610.2026. For the ^{1}H-NMR assignment of anomeric peaks, the spectra were

compared with published aminoethyl 3,6-di-*O*-α-D-mannopyranosyl-α-D-mannopyranoside: $\delta_{H\text{-}1}$: 5.05 ($J_{1,2}$ = 1.6 Hz), $\delta_{H\text{-}1'}$: 4.84 ($J_{1',2'}$ = 1.6 Hz), $\delta_{H\text{-}1''}$: 4.79 (app s).[12] The corresponding ^{13}C signals were assigned through heteronuclear coupling obtained by HSQC NMR experiment. Regarding the measurement of the $[\alpha]_D^{25}$, reported values for similar mannotriosides by Oscarson *et al.*[9] are in the +86 to +100cross range, which is in agreement with the value but disagreement with the sign of the data hereby reported. More literature is needed to have a more conclusive comparison, however, these are the only examples of published mannotriosides.

Bovine serum albumin conjugates synthesis

Propargyl-BSA (7)

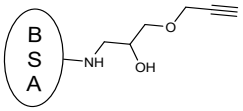

BSA (31.4 mg, 4.7 µmol,1 eq.) was dissolved in 3 mL of 10 mM aqueous solution of $NaHCO_3$, and equally divided in three eppendorf tubes. 5 µL of glycidyl propargyl ether were added to each vial under the fume hood. The vials were closed, protected from light with aluminium foil and put in a heating block at 37 °C to react overnight without stirring. The crude reaction mixture was dialysed for 48 h, changing the dialysis mili-Q water after 24 h, allowing to purify conjugate **7**.

The characterisation of propargyl-BSA was performed *via* differential average mass observed in MALDI-ToF (**Figure S1**), data shown in **Table 1**.

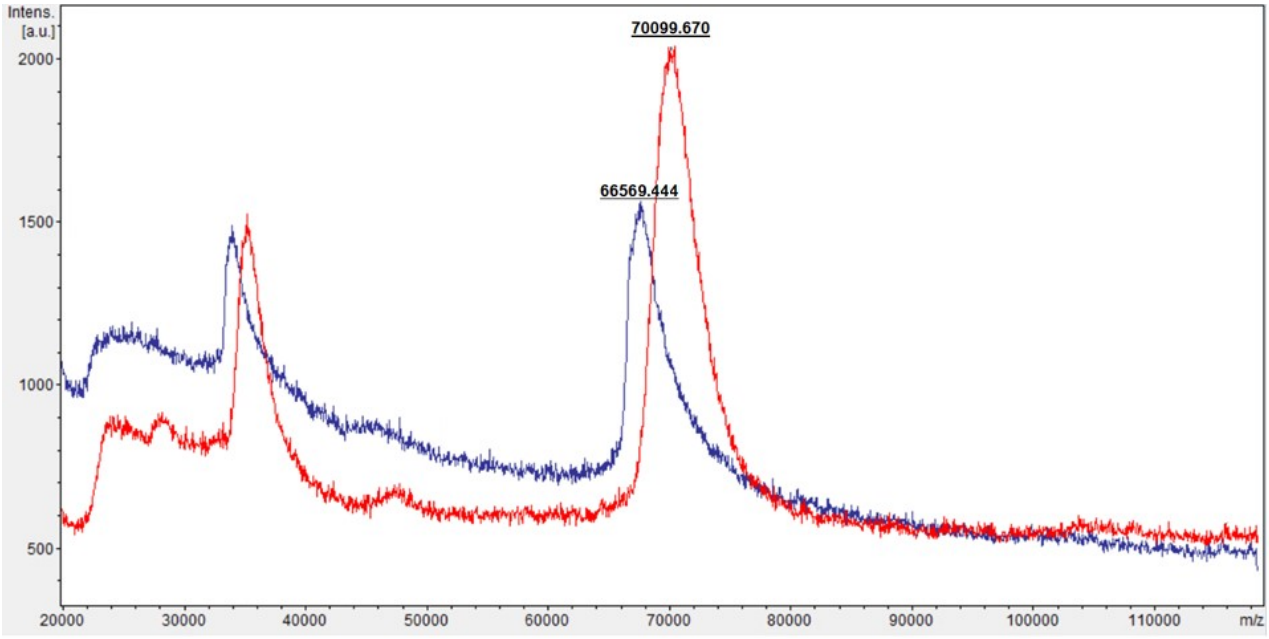

Figure S1. MALDI-ToF data corresponding to propargyl-BSA (**7**) (red) in comparison with BSA (blue).

General method for glycan-BSA conjugate synthesis (8-13)

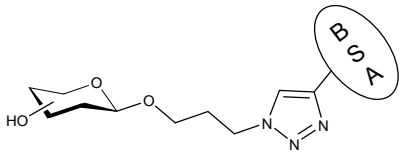

For the copper-catalysed azide-alkyne cycloadditions, stock aqueous solutions of the azidopropyl glycoside (50 mM), propargyl-BSA **7** (10 mg/mL), copper sulphate (1 M), tris-hydroxypropyltriazolylmethylamine (THPTA, 1 M) were used. Freshly prepared 1 M aqueous solution of sodium ascorbate was used. THPTA (10.99 µL) and copper sulphate (4.39 µL) were mixed (solution A). Propargyl-BSA (**7**, 1 mg) was added to a 2 mL eppendorf tube and was then dissolved in 1 mL of mili-Q water. Following vortexing, the glycoside was added and the mixture was vortexed again. Shortly after, solution A was added to the eppendorf tube. Finally, sodium ascorbate (1.12 µL) was added to the mixture and the reaction was vortexed and set in a heating block at 37 ºC overnight without stirring. The reaction crude was then dialysed for 24 h and the glycoconjugate was freeze-dried, redissolved in water to 1 mg/mL concentration and stored at -20 ºC.

The average number of glycans installed on BSA was evaluated according to the difference in molecular weight before and after the conjugation as observed in the reported MALDI-ToF spectra, (**Figures S2-8**), data are reported in **Table 1**.

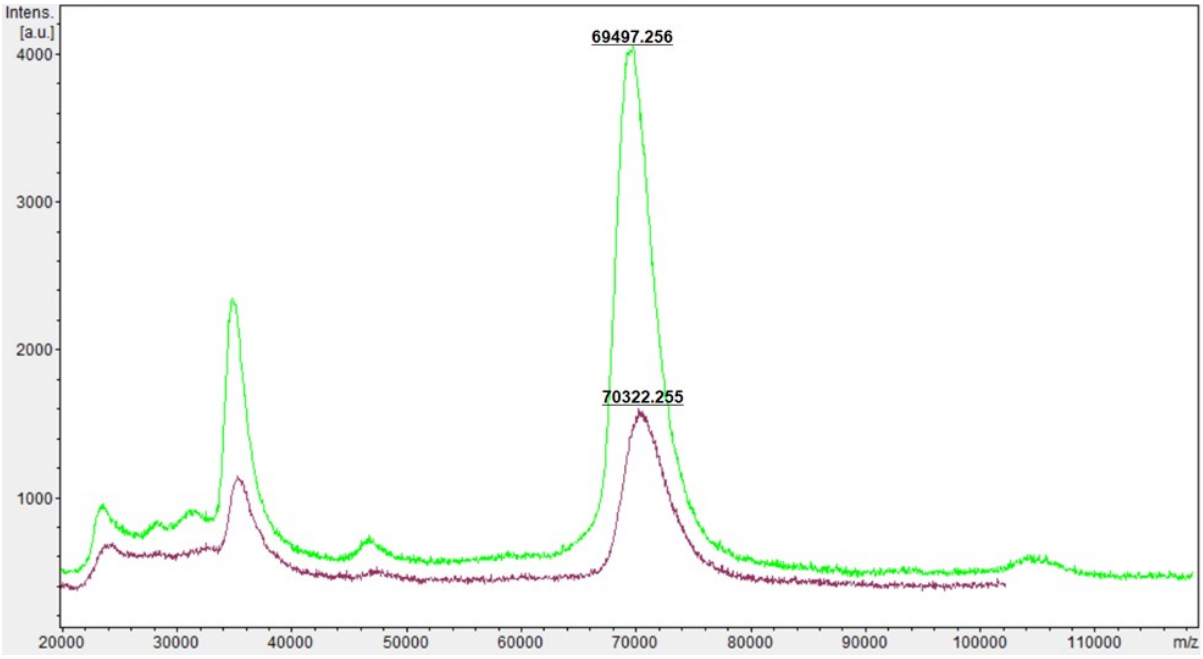

Figure S2. MALDI-ToF data corresponding to Gal-BSA (**8**) (purple) in comparison with propargyl-BSA (**7**) (green).

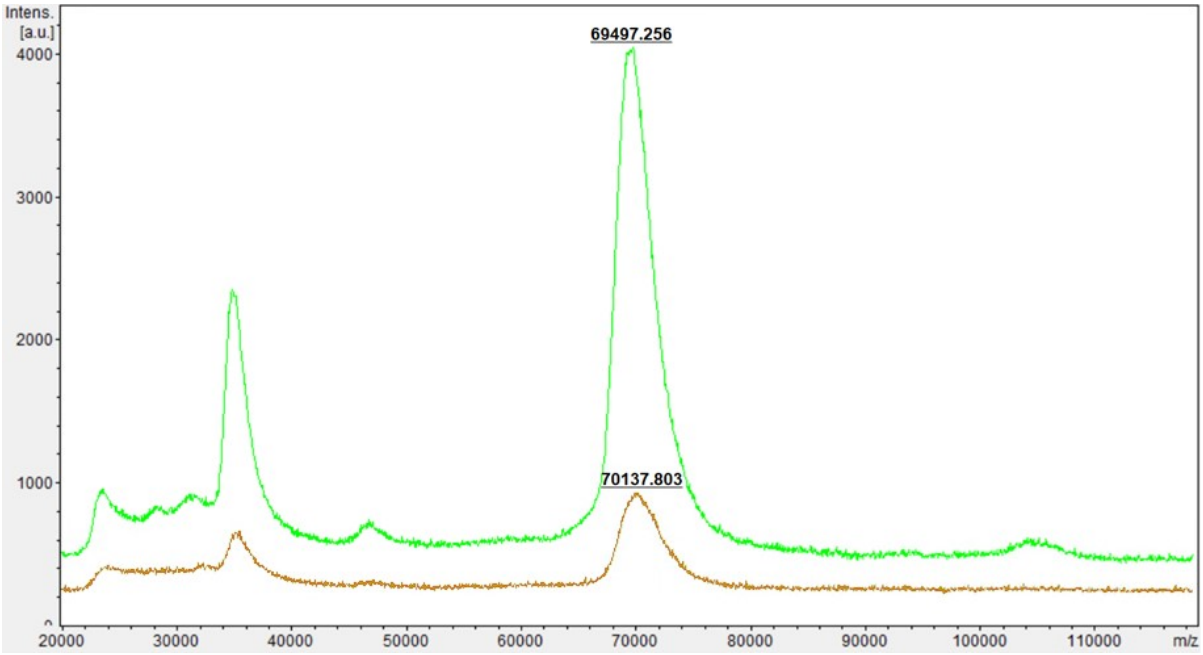

Figure S3. MALDI-ToF data corresponding to Lac-BSA (**9**) (brown) in comparison with propargyl-BSA (**7**) (green).

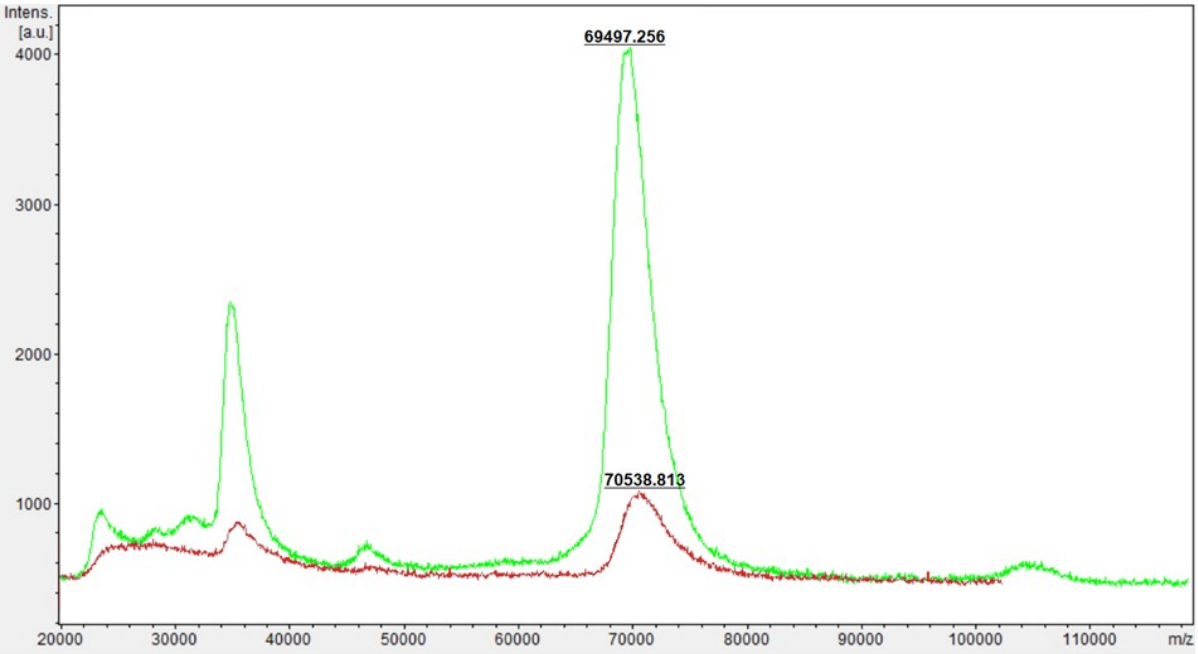

Figure S4. MALDI-ToF data corresponding to Glc-BSA (**10**) (red) in comparison with propargyl-BSA (**7**) (green).

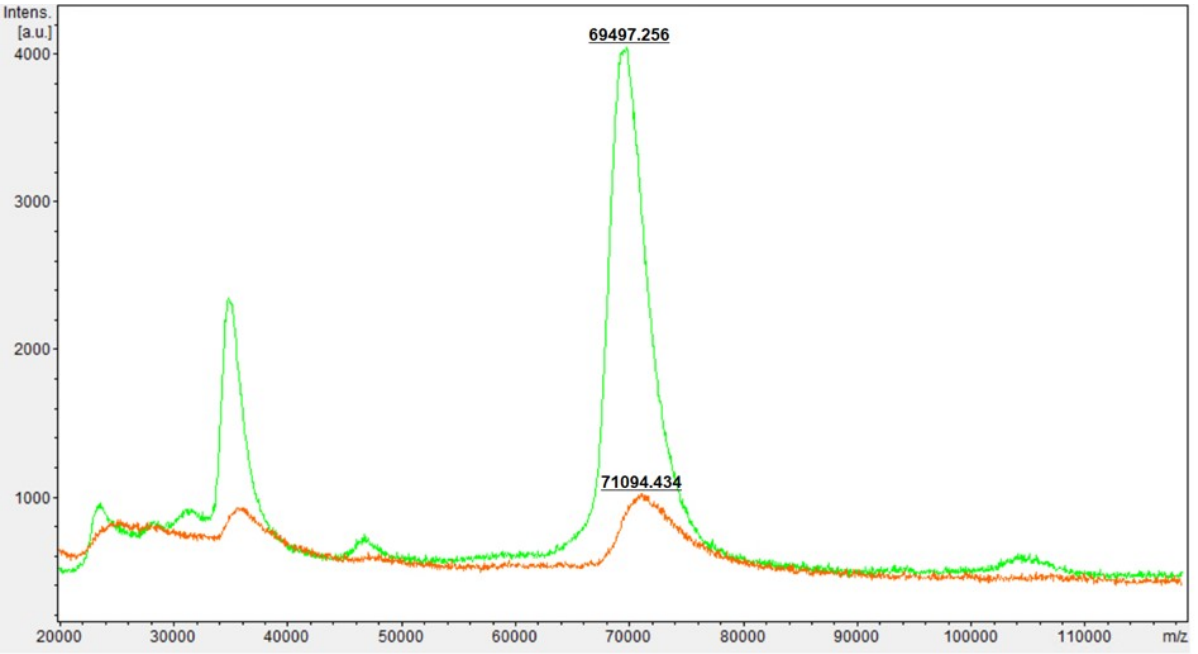

Figure S5. MALDI-ToF data corresponding to Man-BSA (**11**) (orange) in comparison with propargyl-BSA (**7**) (green).

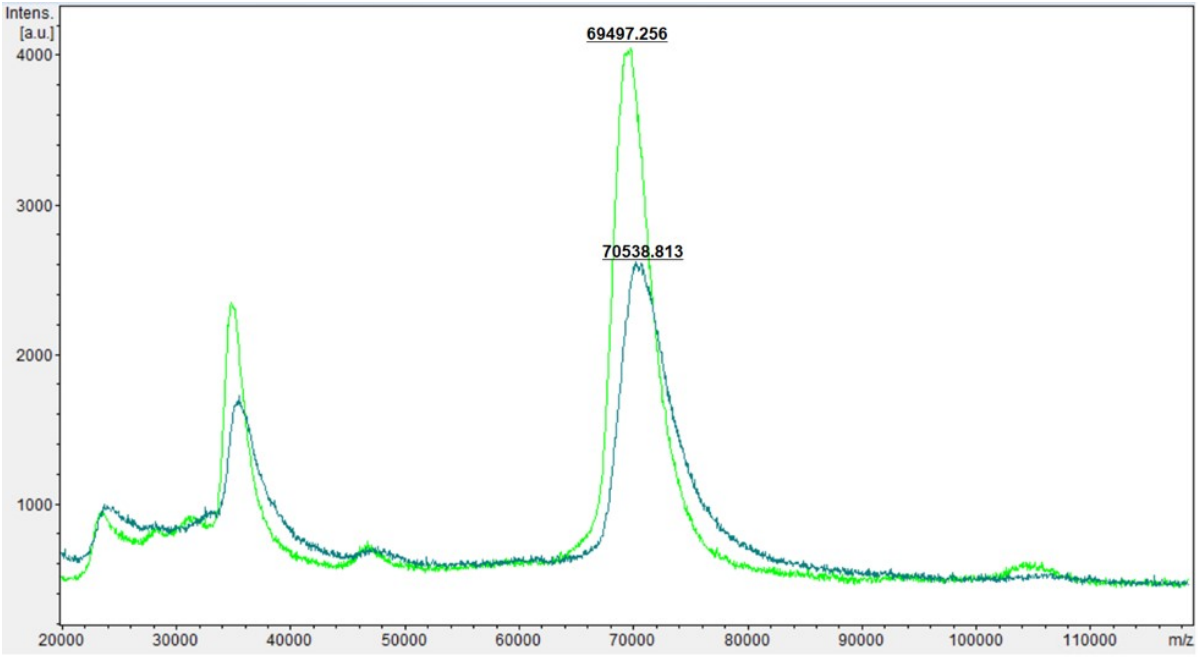

Figure S6. MALDI-ToF data corresponding to α3α6-BSA (**12**) (dark green) in comparison with propargyl-BSA (**7**) (green).

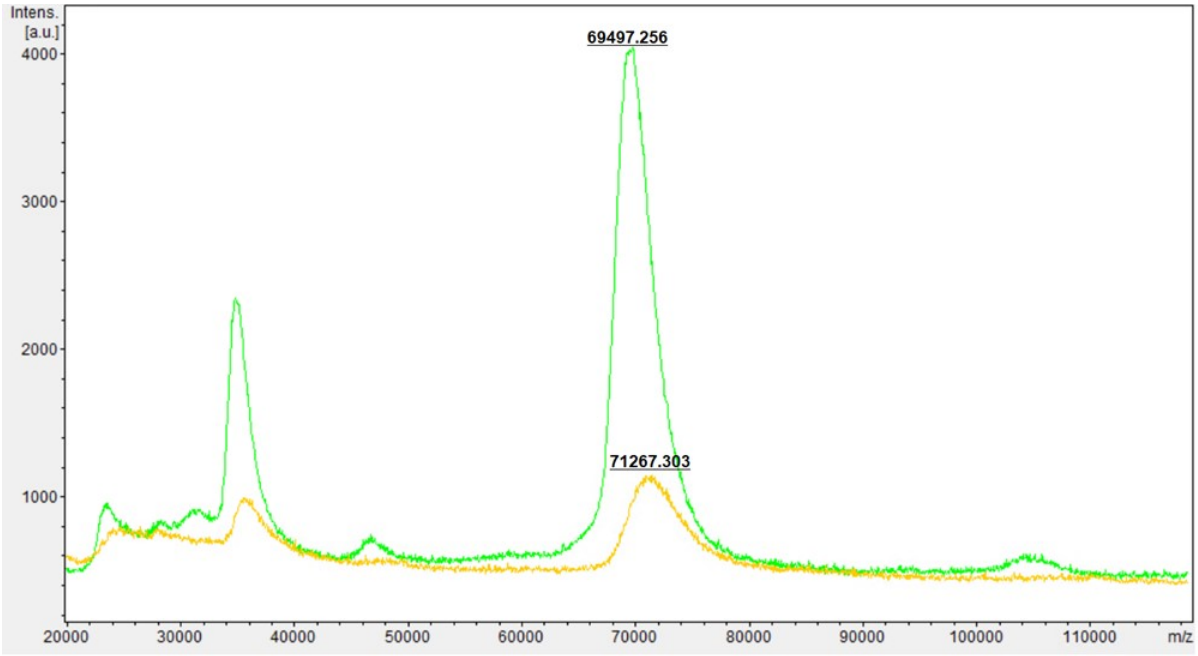

Figure S7. MALDI-ToF data corresponding to 3'SL-BSA (**13**) (yellow) in comparison with propargyl-BSA (**7**) (green).

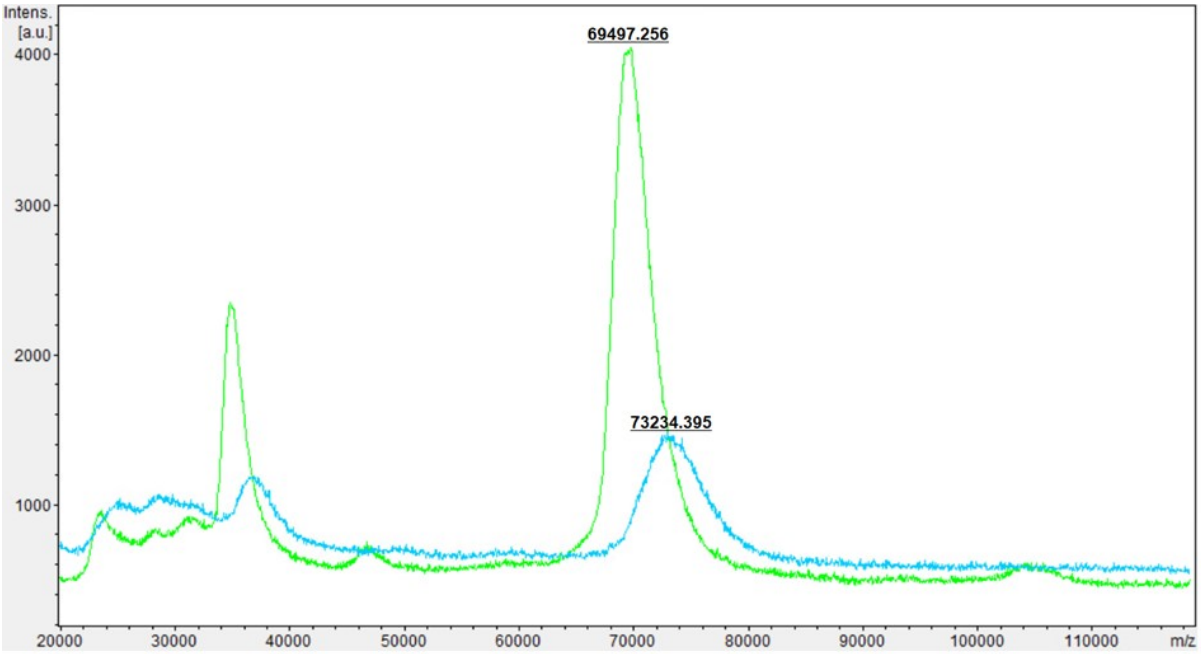

Figure S8. MALDI-ToF data corresponding to Gal_{14}-BSA (**8a**) (light blue) in comparison with propargyl-BSA (**7**) (green).

Passive adsorption on 40 nm AuNPs

General method for passive adsorption (14-20)

A solution of the required BSA conjugate was prepared in citric acid buffer 2 mM pH 5.3 (200 µL, 250 µg/mL). Tween-20 (5 µL, 1% (w/v)) was added to 100 µL of 40 nm AuNPs (Expedeon, OD 10). The nanoparticles were spun down in a Techne Genofuge 16M microcentrifuge (R = 73 mm, 1,650 xg, 10 min). The pellet of the nanoparticles was resuspended in the BSA adduct solution. This mixture was gently pipette-mixed several times. The reaction was set in a rotating mixer at gentle speed for one hour at room temperature, then protected from light with aluminium foil and left still at room temperature overnight. Next day, tween-20 (1 µL, 10% (w/v)) was added. The AuNPs were pelleted and resuspended in 200 µL of PBT (10 mM, pH 7.4) three times. Finally resuspended in 100 µL PBT and the OD was measured at 527.

TEM images of a selection of particles (citrate-capped AuNPs, propargyl-BSA-AuNPs and Gal-BSA-AuNPs are shown in **Figure S9A**. The characterisation of all BSA-AuNPs was performed *via* UV-Vis absorption and DLS, data shown in **Table S3** and **Figure S9B-C**.

Table S3. Characterisation data for all the BSA-AuNPs synthesised in this work.

Particle	Ligand	λ_{max} ± h/2 (nm)	Diameter (nm)
cit-AuNP	Citrate	527 ± 32	33.6 ± 0.9
Propargyl-BSA-AuNP (**14**)	Propargyl-BSA	527 ± 32	40.9 ± 0.6
Gal-BSA-AuNP (**15**)	Gal-BSA	527 ± 32	41.9 ± 0.9
Lac-BSA-AuNP (**16**)	Lac-BSA	527 ± 32	42.2 ± 0.4
Glc-BSA-AuNP (**17**)	Glc-BSA	527 ± 32	41.4 ± 0.6
Man-BSA-AuNP (**18**)	Man-BSA	527 ± 32	41.0 ± 0.3
α3α6Man-BSA-AuNPs (**19**)	α3α6Man-BSA	527 ± 32	42.6 ± 0.6
3'SL-BSA-AuNPs (**20**)	3'SL-BSA	527 ± 32	42.0 ± 0.8
Gal_{14}-BSA-AuNP (**15a**)	Gal_{14}-BSA	527 ± 32	38.9 ± 0.6
NHS-AuNP	NHS ester	530 ± 34	59.6 ± 0.5
propyl-AuNP (**23**)	Propyl	530 ± 34	63.5 ± 1.5
Gal-AuNP (**22**)	Gal	530 ± 34	59.6 ± 0.5
NHS-AuNS	NHS ester	800 ± 186	149.6 ± 0.4
propyl-AuNS (**25**)	Propyl	800 ± 186	149.6 ± 0.4
Gal-AuNS (**24**)	Gal	800 ± 186	149.6 ± 0.4

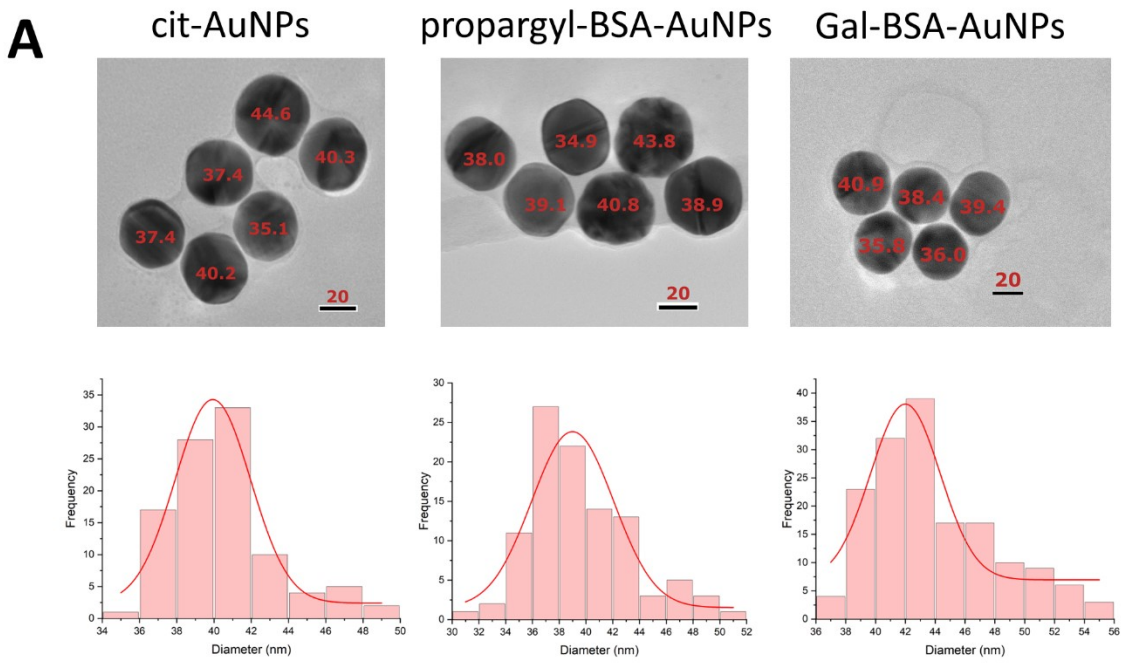

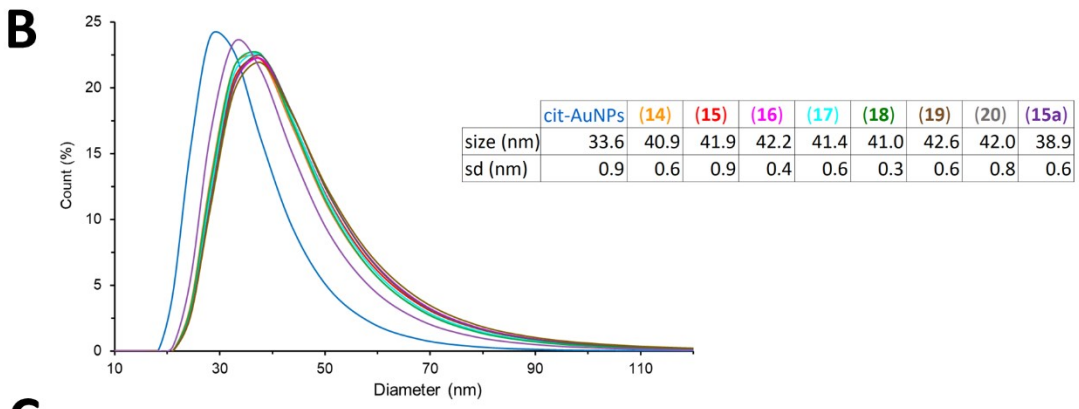

	cit-AuNPs	(14)	(15)	(16)	(17)	(18)	(19)	(20)	(15a)
size (nm)	33.6	40.9	41.9	42.2	41.4	41.0	42.6	42.0	38.9
sd (nm)	0.9	0.6	0.9	0.4	0.6	0.3	0.6	0.8	0.6

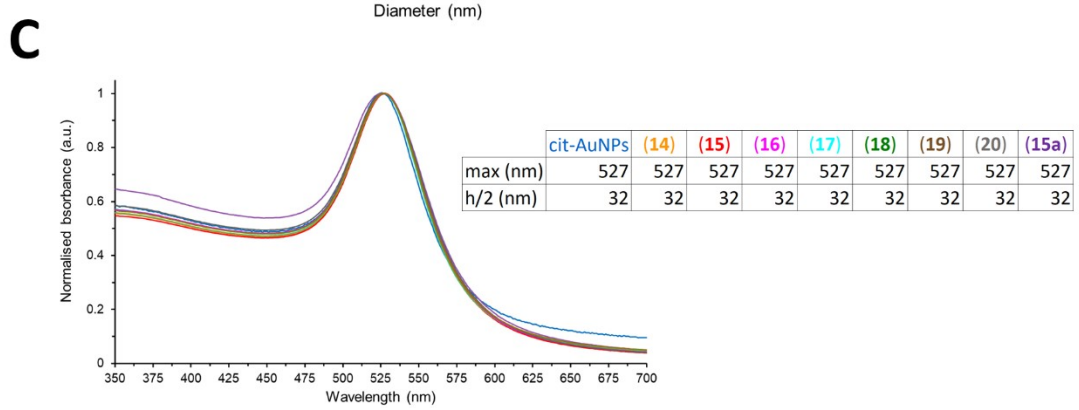

	cit-AuNPs	(14)	(15)	(16)	(17)	(18)	(19)	(20)	(15a)
max (nm)	527	527	527	527	527	527	527	527	527
h/2 (nm)	32	32	32	32	32	32	32	32	32

Figure S9. Characterisation of BSA-AuNPs synthesised in this work. **(A)** Representative TEM images of cit-AuNPs, BSA-AuNPs (**14**), and Gal-AuPSs (**15**), with the value of the estimated measurement of the diameter in red for each nanoparticle. Below, the corresponding size histogram. **(B)** Characterisation of the citrate-AuNPs and functionalised nanoparticles **14-20** by DLS. **(C)** Characterisation of the citrate-AuNPs and functionalised nanoparticles **14-20** by UV-Vis.

Covalent binding to 150 nm AuNSs and 40 nm AuNPs

General method for covalent binding (22-25)

A lyophilised reaction kit (NanoComposix for 150 AuNSs / CytoDiagnostics for 40 nm AuNPs, equivalent to 100 µL OD 20) was allowed to room temperature (20 minutes). A 500 µL solution of the aminopropyl galactoside **21** was prepared in HEPES-PEG reaction buffer (0.1 M pH 8 and 0.5% (w/v) PEG-20K). The defrosted nanoshells were resuspended in 500 µL of HEPES-PEG buffer and transferred to the glycoside solution. The reaction tube was kept in the rotating mixer at gently rotation speed at room temperature for 6 hours, after which it was quenched with 10.8 µL of propylamine. The mixture was centrifuged in a Techne Genofuge 16M microcentrifuge (R = 73 mm, 2,200 xg, 15 minutes). The pellet was resuspended in 200 µL of reaction buffer. The centrifugation and resuspension in reaction buffer steps were repeated three times in total. The pellet was finally resuspended in 100 µL of the conjugate diluent (10 mM PBS, 0.5 % (w/v) BSA, 0.5% (w/v) Tween-20, 0.05% (w/v) NaN_3) to have an OD 20 solution of the functionalised AuNSs or AuNPs.

The characterisation of all the covalently-functionalised AuNPs and AuNSs was performed *via* TEM, UV-Vis absorption and DLS. Data are reported shown in **Table S4** and **Figure S10**.

Table S4. Characterisation data for all the covalently functionalised AuNPs and AuNSs synthesised in this work.

Particle	Ligand	$\lambda_{max} \pm h/2$ (nm)	Diameter (nm)
NHS-AuNP	NHS ester	530 ± 34	50.7 ± 0.5
propyl-AuNP (**23**)	Propyl	530 ± 34	50.7 ± 1.5
Gal-AuNP (**22**)	Gal	530 ± 34	58.8 ± 0.5
NHS-AuNS	NHS ester	800 ± 186	142.1 ± 0.4
propyl-AuNS (**25**)	Propyl	800 ± 186	142.1 ± 0.4
Gal-AuNS (**24**)	Gal	800 ± 186	149.6 ± 0.4

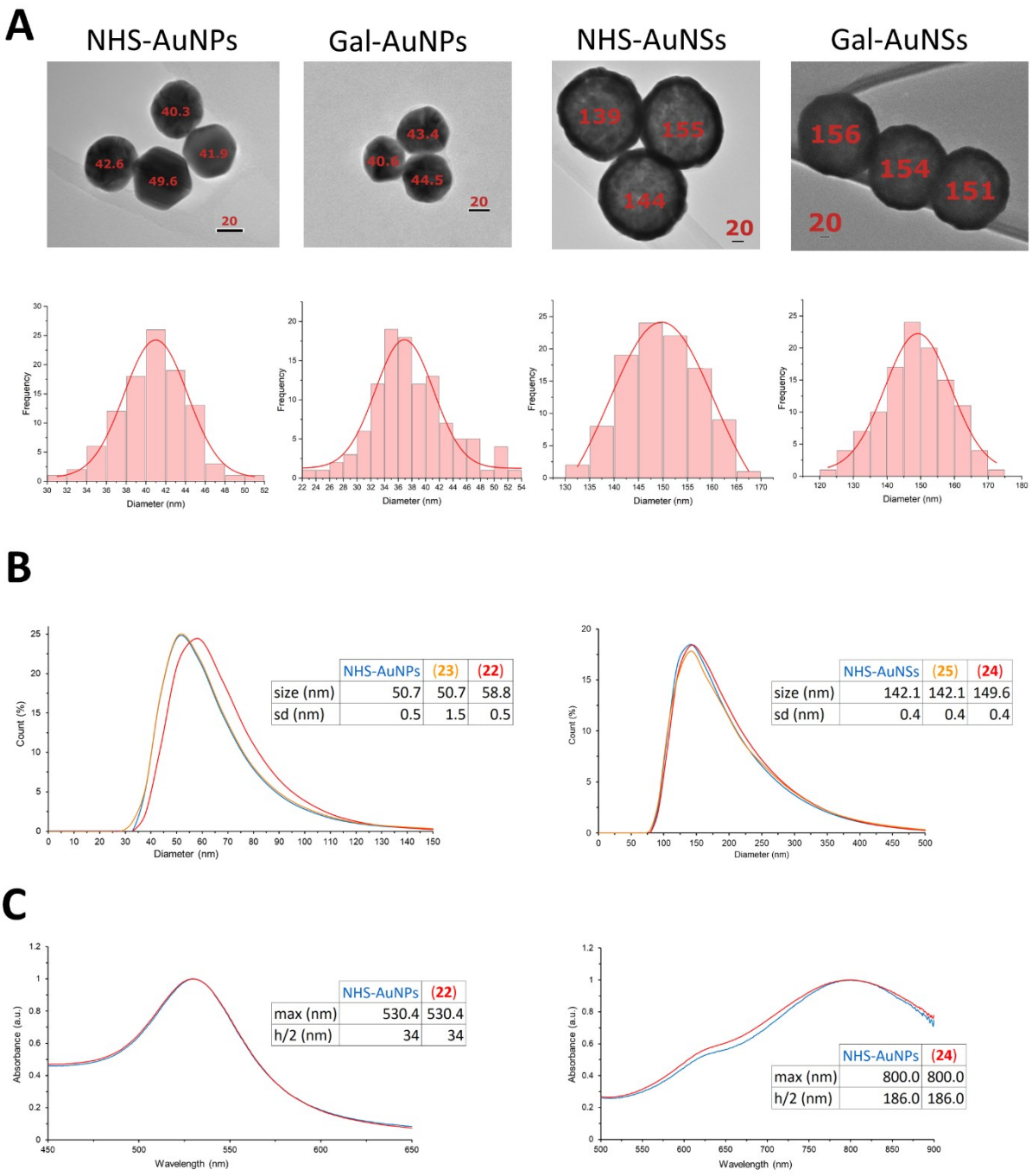

Figure S10. Characterisation of covalently functionalised AuNPs and AuNSs synthesised in this work. **(A)** Selection of TEM images forNHS-AuNPs, Gal-AuNPs (**22**), NHS-AuNSs and Gal-AuNSs (**24**), with the value of the estimated measurement of the diameter in red for each nanoparticle.. Below, the TEM distribution corresponding to each type of nanoparticle. **(B)** Characterisation of the commercial NHS-AuNPs and functionalised AuNPs **23-22** and **25-24** by DLS. **(C)** Characterisation of the functionalised commercial NHS-AuNPs and functionalised AuNPs **22** and **24** by UV-Vis.

Assessment of nanoparticle performance *via* dipstick assay

The correct functionalisation and the efficiency of both gold nanoparticles and nanoshells were investigated by their performance using a dipstick assays format. A dipstick consists in a simplified version of a lateral flow device. A schematic representation is shown in **Figure S11A** and it is formed by three components. A nitrocellulose layer with specific characteristics such as the content of surfactant, the porosity, and thickness. On top of the nitrocellulose strip, the cotton wick is generating a pulling force to allow the sample to flow through the nitrocellulose strip. The nitrocellulose and the wick are supported by an underlying a layer of a plastic adhesive backing card holding all the components. Unless differently specified, the usual nitrocellulose employed for the assays was Immunopore RP-90-150. Once assembled the dipsticks are stored under dry conditions in a Falcon tube containing a desiccant pouch. Slightly higher than the middle of the nitrocellulose strip, 0.5 µL of a specified concentration of a selected lectin is deposited as a test spot (**Figure S11B**). The assay performed using a dipstick system consists of four steps (**Figure S11C**). In a microfuge tube, 20 µL of stock solution of dipstick buffer, consisting of 10 mM PB, 1% PVP, 50 mM NaCl and 0.05% Tween-20, are added. The corners of the lower edge of the dipstick are cut to give a sharp shape, and the dipstick is introduced in the microfuge tube containing the dipstick buffer. The solution is allowed to travel along the nitrocellulose conditioning the strip. In the following step the dipstick is transferred to a second microfuge tube containing 20 µL of running solution. The composition of the running solution is, unless specified differently, OD 1 AuNPs, 10 mM PB, 1% (w/v) PVP, 50 mM NaCl, 0.05% (w/v) Tween-20 for AuNPs, or OD 1 AuNSs, 10 mM PB, 1% (w/v) PVP, 150 mM NaCl 1% (w/v) Triton X100 and 1% (w/v) BSA for AuNSs. The second run was left for 10 minutes, after which the presence or absence of the coloured spot can be observed. The signal intensities were quantified with a gel electrophoresis imager Chemidoc (Biorad).

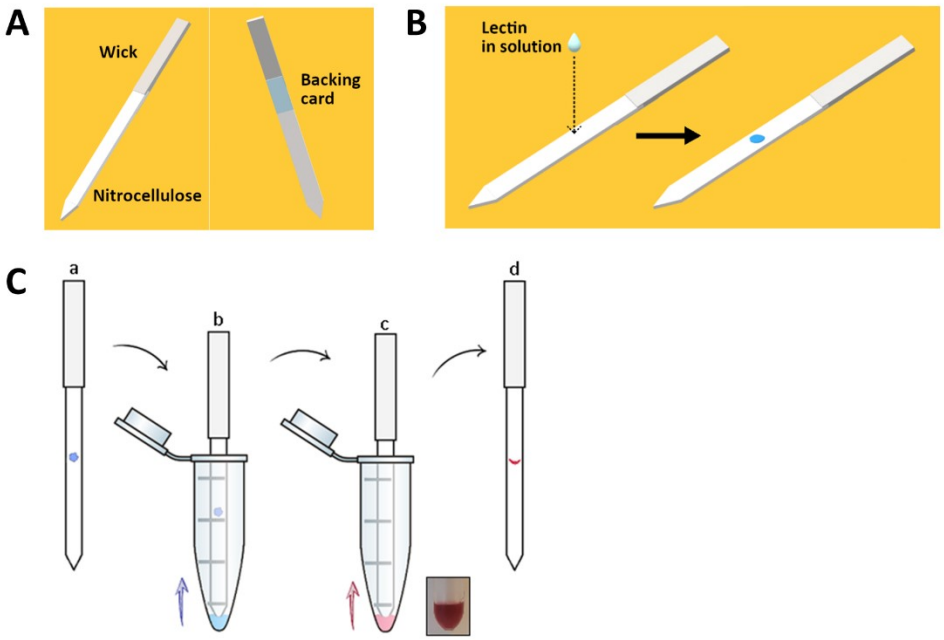

Figure S11. (**A**): (*left*) schematic representation of the dipstick front and (*right*) backside. (**B**): an aqueous solution containing the lectin of interest (typically 0.5 µL at a concentration of 5 mg/mL) is spotted on the nitrocellulose strip. (**C**): workflow scheme of the dipstick assay, starting with (**a**) depositing the lectin, (**b**) eluting 20 µL of running buffer to condition the strip, (**c**) eluting the solution of nanoparticles in dipstick buffer and (**d**) development of the signal, typically red-coloured due to the plasmon resonance absorbance of 40 nm AuNPs. The inset shows a photographic image of an Eppendorf vial containing AuNPs at OD 1.

Functionalisation of gold nanoparticles and gold nanoshells: optimisation and resolution of unspecific interactions

The glyconanoparticles synthesised following the BSA-approach did not exhibit any non-specific interactions. The dipsticks corresponding to the propargylated BSA-AuNPs, Gal-BSA-AuNPs and Lac-BSA-AuNPs are shown in **Figure S12**.

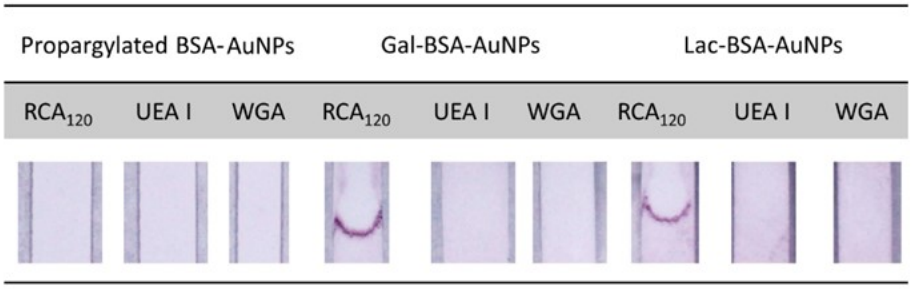

Figure S12. Dipstick assay for the detection of RCA_{120} (2.5 µg) with Gal-BSA-AuNPs and Lac-BSA-AuNPs**.** Negative controls include the 2'-fucoside-binding UEA I and the sialic acid-binding WGA (2.5 µg each). The propargylated BSA-AuNPs were also assayed to probe the absence of non-specific interactions with either of the lectins. The assay was repeated in triplicates, obtaining similar results.

The glyconanoshells synthesised through NHS ester coupling required a different buffer (see *Assessment of nanoparticle performance via dipstick assay* section above) to avoid non-specific interactions. The reaction conditions (incubation time, pH and glycoside concentration) for the functionalisation of gold nanoshells were optimised to 6 h, pH 8 and glycoside 1 mM (**Figure S13**).

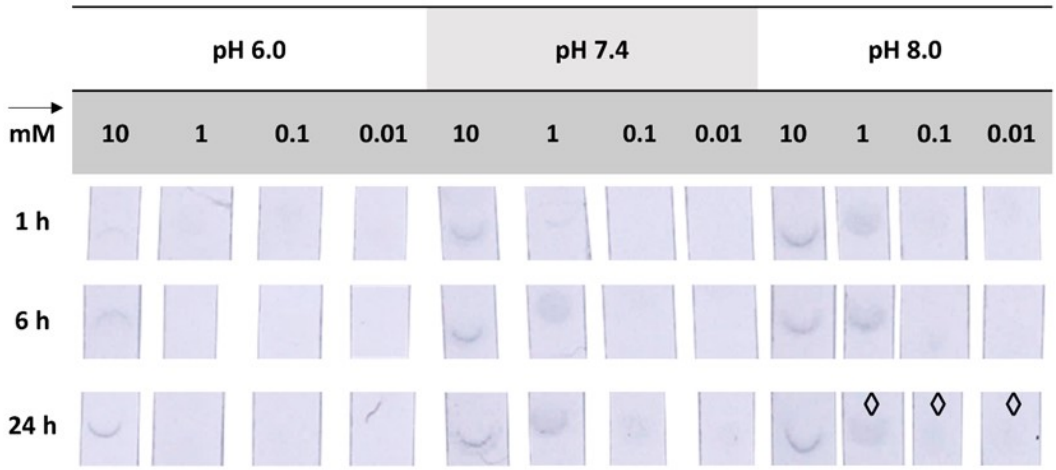

Figure S13. Optimisation of the NHS coupling between 3-aminopropyl galactoside (**21**) and NHS ester-activated AuNSs and AuNPs. The results of the optimisation were analysed through the detection of RCA_{120} (2.5 µg) with OD 1 of the AuNSs **24** synthesised. with the functionalisation was screened at different concentrations of **21** (10, 1, 0.1, 0.01 mM), at different pHs (6.0, 7.4, 8.0) and over different incubation times (1, 6, 24 h). ◊: indicates aggregation of the AuNSs at the bottom of the dipstick.

Using the same conditions, NHS-activated gold nanoparticles were functionalised following a similar pathway, only optimising the concentration of glycoside required (**Figure S14**), which was 0.1 mM.

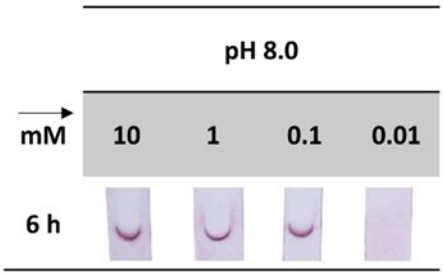

Figure S14. Dipstick signals for the detection of RCA_{120} with glyconanoparticles functionalised with different concentrations of **21** (10, 1, 0.1, 0.01 mM), at pH 8.0 over 6 h.

The glyconanoparticles (both AuNSs and AuNPs) synthesised through this method did not exhibit non-specific interactions (**Figure S15**).

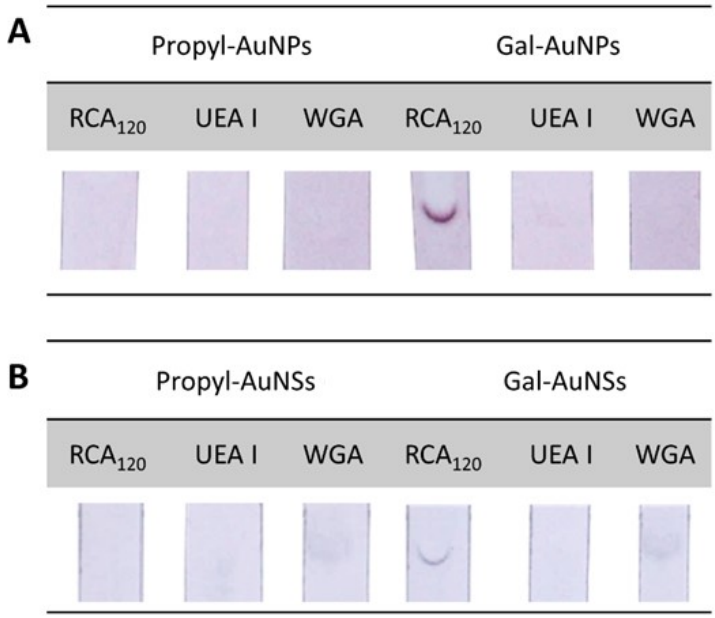

Figure S15. Dipstick assay under optimised conditions for the detection of RCA_{120} (2.5 µg) with (**A**) Gal-AuNPs and (**B**) Gal-AuNSs. Negative controls include the 2'-fucoside-binding UEA I and the sialic acid-binding WGA (2.5 µg each). The propyl-AuNPs and propyl-AuNSs were also assayed to probe the absence of non-specific interactions with either of the lectins. The assay was repeated in triplicates, obtaining similar results.

Attempts to improve the sensitivity *via* increasing the nanoparticle concentration in the dipstick assay

Attempting to improve the limit of the detection, the Gal-BSA-AuNPs (**15**) and Gal-AuNSs (**24**) were tested at OD 5 instead of OD 1 for the detection of RCA_{120}. Whereas **15** did not present any particular complication, **24** aggregated at the bottom of the dipstick in every test. To solve the issue, different nitrocellulose membranes were tested for the assembly of the dipstick. Three main characteristics define the performance of a nitrocellulose strip: flow speed (s/strip), thickness (µm) and content of surfactant in the strip. A series of experiments were performed to investigate the influence of the flow speed of the nitrocellulose employed to assemble the dipstick (**Figure S16**). For that set of experiments, neither slow (entry 1) nor medium flow speed (entries 2-5, being 2 the one used by default in this paper) prevented the aggregation of glyconanoshells at the bottom of the dipstick. Higher speeds (entries 6-9) partially avoided the aggregation and a signal indicating the detection of the lectin could be observed, especially for entry 9. The best result was obtained when using nitrocellulose with the highest speed (entry 10), which seemed to recover the signal for the detection of RCA_{120}.

Given that the type and content of surfactants in the different types of nitrocellulose are not disclosed by the manufacturers, they will not be compared in this study.

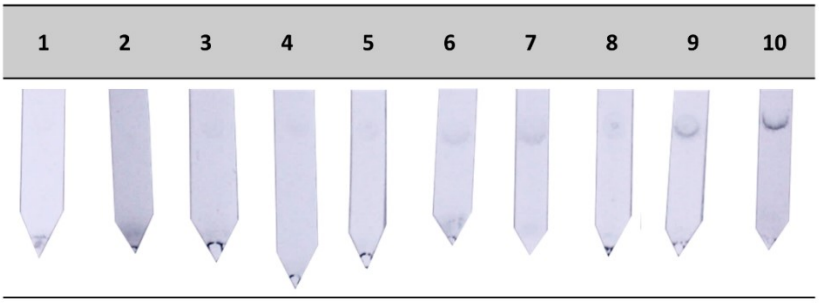

Figure S16. Influence of the nitrocellulose to overcome the aggregation of AuNSs at OD 5 in the dipstick assay. Gal-AuNSs (**24**) at OD 5 were used to detect RCA_{120} (2.5 µg). The types of nitrocellulose tested included **1**: Immunopore FP (110-150 s/strip, 200 µm thick). **2**: Immunopore RP (90-150 s/strip, 200 µm thick); **3**: FF120HP (90-150 s/strip, reduced content of surfactant, 200 µm thick); **4**: FF120HP Plus (90-150 s/strip, higher content of surfactant, 200 µm thick); **5**: FF120HP Plus Thick (90-150 s/strip, higher content of surfactant, 235 µm thick); **6**: Immunopore XP (60-100 s/strip, 200 µm thick); **7**: FF80HP (90-150 s/strip, reduced content of surfactant, 200 µm thick); **8**: FF80HP Plus (90-150 s/strip, higher content of surfactant, 200 µm thick); **9**: FF80HP Plus Thick (90-150 s/strip, higher content of surfactant, 235 µm thick); **10**: Prima40 (40 s/strip, higher content of surfactant, unknown thickness).

With the issue of aggregation solved, the sensitivity assay was repeated using the usual *Immunopore RP* nitrocellulose (entry 2) for Gal-BSA-AuNPs **15** and *Prima 40* (entry 10) for Gal-AuNSs **24** (**Figure S17**). A remarkable increase in the intensity of the signal could be appreciated, whereas, unfortunately, the sensitivity remained unchanged.

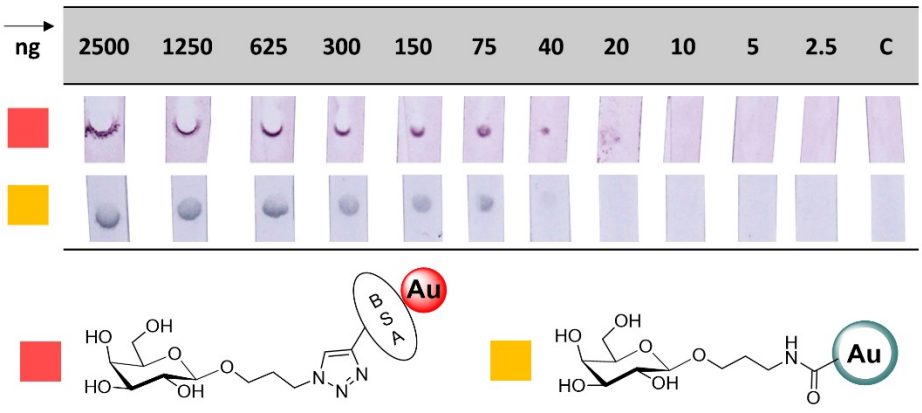

Figure S17. Sensitivity studies using OD 5 of either Gal-BSA-AuNPs (**15**) or Gal-AuNSs (**24**) for the detection of RCA_{120} ranging from 2500 – 2.5 ng in a dipstick assay. C: negative control performed with the respective propyl-functionalised particles (**14** or **25**) for the detection of 2500 ng of RCA_{120}.

Trypanosoma cruzi **trans-sialidase expression and purification**

Adapted from Harrison *et al.*[13] For this study, 10 mL of ampicillin (10 µL of 100 mg/mL) supplemented LB medium were inoculated from cryo-glycerol stocks and incubated overnight at 37 °C with shaking at 200 rpm.

1 mL of this culture was used to inoculate 100 mL of ampicillin (100 µL of 100 mg/mL) supplemented LB medium, which was incubated at 37 °C with orbital shaking at 200 rpm overnight. 20 mL of this culture were used to inoculate 1 L of ampicillin (1 mL of 100 mg/mL) supplemented LB medium, which was incubated at 37 °C for 4 h with orbital shaking at 200 rpm until it reached an OD_{600nm} of 1. The culture was then induced with 0.2 mM isopropyl β-D-1-thiogalactopyranoside (IPTG, 200 µL of 1M) and incubated overnight at 18 °C.

Lysis and purification

The culture was centrifuged at 12,000 × g at 4 °C for 20 minutes, and the pellets harvested for lysis. The pellets were suspended in B-PER complete bacterial protein extraction reagent, (Termofisher).

5 mL of B-PER were added per gramme of the pellets, followed by Protease Inhibitor cocktail (final concentration 2 mM benzamidine, 2 mM pepstatin, 2 mM leupeptine, 10 µL of solution per mL of suspension) and lysozyme (50 mg/ml stock solution, 10 µL per ml of suspension, for a final concentration of 250 µg/mL)

The suspension was incubated for 30 minutes at room temperature under gentle mixing and centrifuged at 4000 x g, 4 °C, for 20 min and the supernatant was collected.

Purification of the Enzyme by Immobilized Metal Ion Affinity Chromatography IMAC

Purification of the enzyme was performed from *E. coli* soluble extracts containing enzyme, using a 1-mL-column HisTrap™ High Performance (Cytiva).

Following cell lysis and centrifugation, the supernatant was transferred into a 1 mL HisTrap HP column cartridge and the following purification protocol was performed using an AKTA-FPLC equipped with an UV detector. Using a flow of 1 mL/min, the column was washed with 5 CV of cold buffer A (20 mM imidazole, 0.5 M NaCl, 50 mM glycine, 50 mM TRIS-HCL, pH 8).

Elution was performed using 5 CV of cold buffer B (200 mM imidazole, 0.5 M NaCl, 50 mM glycine, 50 mM TRIS-HCL, pH 8). The purified fractions 18-22 were collected and pooled together (**Figure S18**). The column was finally regenerated with 5 CV of buffer B, and re-equilibrated with 5 CV of buffer A.

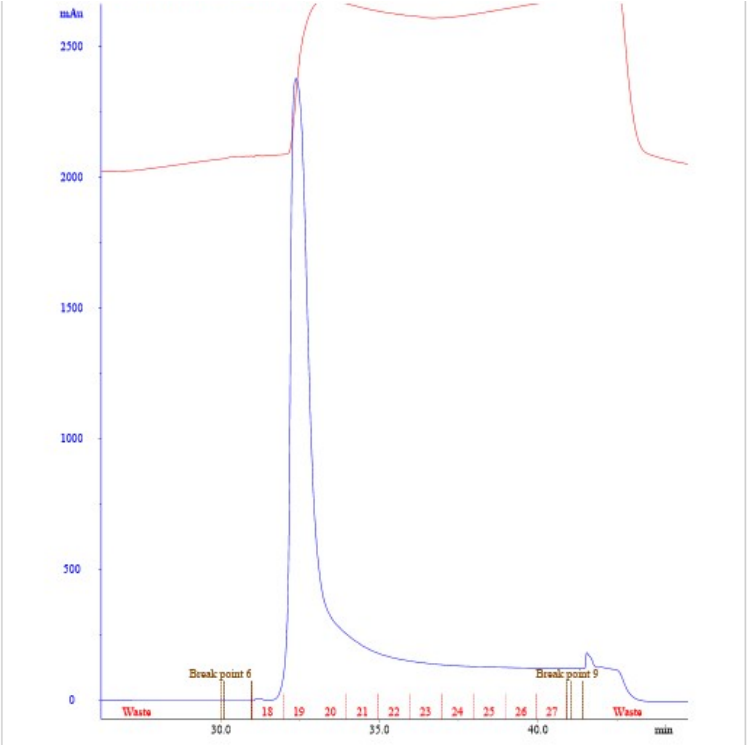

Figure S18. Elution profile of the His-Trap purification step

The eluates were desalted by gel filtration chromatography, using a NAP-10 column (Sephadex G-25 Medium; Sigma) to eliminate the imidazole and evaluated by SDS-PAGE (**Figure S19**). The mass of protein obtained was 4.73 mg.

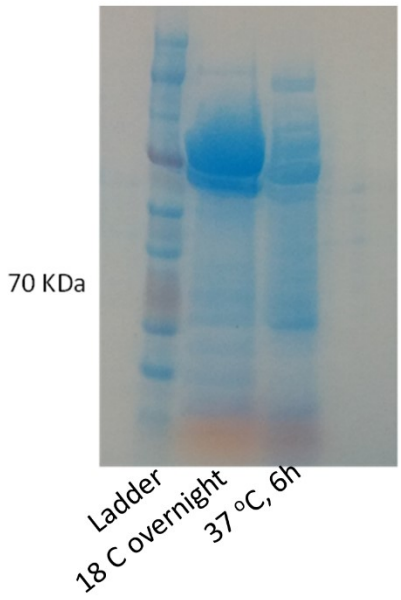

Figure S19. SDS gel analysis of purified lysate (18 °C overnight) and aliquot taken after incubation at 37 °C for 6 h.

References

1 Z. Y. Zhu, D. Cui, H. Gao, F. Y. Dong, X. C. Liu, F. Liu, L. Chen and Y. M. Zhang, Efficient synthesis and activity of beneficial intestinal flora of two lactulose-derived oligosaccharides, *Eur. J. Med. Chem.*, 2016, **114**, 8–13.

2 C. M. Keyari and R. Polt, Serine and threonine Schiff base esters react with β-anomeric peracetates in the presence of BF3·Et2O to produce β-glycosides, *J. Carbohydr. Chem.*, 2010, **29**, 181–206.

3 Y. Xu, Q. Zhang, Y. Xiao, P. Wu, W. Chen, Z. Song, X. Xiao, L. Meng, J. Zeng and Q. Wan, Practical synthesis of latent disarmed S-2-(2-propylthio)benzyl glycosides for interrupted Pummerer reaction mediated glycosylation, *Tetrahedron Lett.*, 2017, **58**, 2381–2384.

4 M. Tesch, S. Kudruk, M. Letzel and A. Studer, Orthogonal Click Postfunctionalization of Alternating Copolymers Prepared by Nitroxide-Mediated Polymerization, *Chem. Eur. J.*, 2017, **23**, 5915–5919.

5 C. C. Lee, G. Grandinetti, P. M. McLendon and T. M. Reineke, A polycation scaffold presenting tunable 'click' sites: Conjugation to carbohydrate ligands and examination of hepatocyte-targeted pDNA delivery, *Macromol. Biosci.*, 2010, **10**, 585–598.

6 A. Fekete, A. Borbás, S. Antus and A. Lipták, Synthesis of 3,6-branched arabinogalactan-type tetra- and hexasaccharides for characterization of monoclonal antibodies, *Carbohydr. Res.*, 2009, **344**, 1434–1441.

7 A. v. Demchenko and G. J. Boons, A highly convergent synthesis of a complex oligosaccharide derived from group B type III Streptococcus, *J. Org. Chem.*, 2001, **66**, 2547–2554.

8 C. Bensoussan, N. Rival, G. Hanquet, F. Colobert, S. Reymond and J. Cossy, Iron-catalyzed cross-coupling between C-bromo mannopyranoside derivatives and a vinyl Grignard reagent: Toward the synthesis of the C31-C52 fragment of amphidinol 3, *Tetrahedron*, 2013, **69**, 7759–7770.

9 S. Oscarson and A. K. Tidén, Syntheses of the octyl and tetradecyl glycosides of 3,6-di-O-α-d-mannopyranosyl-α-d-mannopyranose and of 3,4-di-O-α-d-mannopyranosyl-α-d-mannopyranose. A new way for 2,4-di-O-protection of mannopyranosides, *Carbohydr. Res.*, 1993, **247**, 323–328.

10 H. Yu, H. Chokhawala, R. Karpel, H. Yu, B. Wu, J. Zhang, Y. Zhang, Q. Jia and X. Chen, A multifunctional Pasteurella multocida sialyltransferase: A powerful tool for the synthesis of sialoside libraries, *J. Am. Chem. Soc.*, 2005, **127**, 17618–17619.

11 W. Y. Lu, X. W. Sun, C. Zhu, J. H. Xu and G. Q. Lin, Expanding the application scope of glycosidases using click chemistry, *Tetrahedron*, 2010, **66**, 750–757.

12 T. K. Lindhorst, K. Bruegge, A. Fuchs and O. Sperling, A bivalent glycopeptide to target two putative carbohydrate binding sites on FimH, *Beilstein J. Org. Chem.*, 2010, **6**, 801–809.

13 J. A. Harrison, K. P. R. Kartha, E. J. L. Fournier, T. L. Lowary, C. Malet, U. J. Nilsson, O. Hindsgaul, S. Schenkman, J. H. Naismith and R. A. Field, Probing the acceptor substrate binding site of Trypanosoma Cruzi trans-sialidase with systematically modified substrates and glycoside libraries, *Org. Biomol. Chem.*, 2011, **9**, 1653–1660.

14 A. R. Todeschini, L. Mendonça-Previato, J. O. Previato, A. Varki and H. van Halbeek, Trans-sialidase from Trypanosoma cruzi catalyzes sialoside hydrolysis with retention of configuration, *Glycobiol.*, 2000, **10**, 213–221.

15 X. Wu, J. Ye, A. T. DeLaitsch, Z. Rashidijahanabad, S. Lang, T. Kakeshpour, Y. Zhao, S. Ramadan, P. V. Saavedra, V. Yuzbasiyan-Gurkan, H. Kavunja, H. Cao, J. C. Gildersleeve and X. Huang, Chemoenzymatic Synthesis of 9NHAc-GD2 Antigen to Overcome the Hydrolytic Instability of O-Acetylated-GD2 for Anticancer Conjugate Vaccine Development, *Angew. Chem. Int. Ed.*, 2021, **60**, 24179–24188.

16 P. T. Nyffeler, C. H. Liang, K. M. Koeller and C. H. Wong, The chemistry of amine-azide interconversion: Catalytic diazotransfer and regioselective azide reduction, *J. Am. Chem. Soc.*, 2002, **124**, 10773–10778.

17 C. Ligeour, L. Dupin, A. Marra, G. Vergoten, A. Meyer, A. Dondoni, E. Souteyrand, J. J. Vasseur, Y. Chevolot and F. Morvan, Synthesis of galactoclusters by metal-free thiol 'click chemistry' and their binding affinities for pseudomonas aeruginosa lectin leca, *Eur. J. Org. Chem.*, 2014, **2014**, 7621–7630.